The geochemical role of B-10 enriched boric acid in cemented liquid radioactive wastes

Mojtaba Rostamiparsa[1] · István Tolnai[2] · Ottó Czömpöly[2] · Margit Fábián[2] · Máté Hegedűs[3] · György Falus[1] · Csaba Szabó[1,4] · Mihály Óvári[2] · Csaba Tóbi[2] · Péter Kónya[5] · Péter Völgyesi[2] · Zsuzsanna Szabó-Krausz[1,6]

Abstract

Boric acid is a significant radioactive waste generated during the operation of nuclear power plants. Cementitious materials have been widely studied for the immobilization of boric acid. The generally used natural boric acid has been replaced by enriched boric acid for geochemical reasons and are expected to have varied behaviors in cementitious matrices. Results showed that simulated enriched/natural boric acid liquid wastes mostly contain boron in $B(OH)_4^-$ and $B_5O_6(OH)_4^-$ ionic forms, but the mass ratio of these species is higher in enriched boric acid solutions. In function with the concentration of enriched/ natural boric acid, the solidified cementitious materials show different mineralogy.

Keywords Cement paste · Molecular geometry · Leaching test · Solidification

Introduction

Boric acid (BA) solutions, due to the high ability of boron in neutron adsorption, are used widely in nuclear technology [1, 2]. Subsequently, BA waste streams are accounted as the main liquid waste residues from nuclear power plants (NPP) under operation[1–8]. These wastes, generally with low to intermediate level of radioactivity, are mostly solidified by different Portland cements enhanced with different mineral and chemical admixtures before subsurface or deep geological deposition [2, 4, 9–12]. The application of cement for such aims is due to the satisfying mechanical, radiation and thermal stabilities of cementitious materials, as well as to the potential of hydrated cement phases (e.g., ettringite) to incorporate borates [4, 9, 13–16] and calcium silicate hydrate (CSH) to build the radionuclides into their structure [17–19]. However, some technical drawbacks of boric acid, such as the corrosive effect inside the operating loops of NPP and the high inherent leachability of boron from final cementitious waste forms had encouraged scientists to find better neutron absorbers [1, 2, 6, 20, 21].

Due to the significant difference between the cross-section of the two boron stable isotopes in thermal neutrons adsorption (σ_{B-10}= 3837 barn and σ_{B-11}= 0.005 barn) [22, 23], some modern NPPs in Germany, France, Japan, India, and the USA have begun to use ^{10}B enriched boric acid (EBA) up to 90% ^{10}B instead of natural boric acid (NBA), which has 20% ^{10}B abundance [1, 2, 24]. This new EBA neutron absorber can provide a more efficient control system during the reactor operation and also produce significantly less waste volume than the use of NBA (the waste volume drops to 30% when EBA with 60% ^{10}B enrichment is applied)[1, 2, 20, 25–27]. However, despite numerous studies on the technical and economic benefits of EBA during the operation of NPP [20, 26, 28], the waste management aspect of this new promising neutron absorber, especially the compatibility of EBA with cementitious matrices has not received attention previously. Meanwhile, isotopic, elemental, and molecular properties of boron are expected to

✉ Margit Fábián
fabian.margit@ek-cer.hu

1 Lithosphere Fluid Research Lab, Eötvös Loránd University, Pazmany P. s. 1/C, Budapest 1117, Hungary

2 Centre for Energy Research, Konkoly-Thege Miklós út. 29-33, Budapest 1121, Hungary

3 Department of Materials Physics, Eötvös Loránd University, Pazmany P. s. 1/C, Budapest 1117, Hungary

4 Institute of Earth Physics and Space Science, Csatkai E. ut. 6-8, Sopron 9400, Hungary

5 Directorate of Geology, Supervisory Authority of Regulatory Affairs, Stefania ut. 14, Budapest 1143, Hungary

6 Centre of Environmental Sciences, Eötvös Loránd University, Pazmany P. s. 1/C, Budapest 1117, Hungary

cause different behaviors of NBA and EBA in cementitious matrices as well as different stability and durability of their final waste forms. The reason is the significant relative mass difference of the ^{10}B and ^{11}B isotopes, and the dependence of borate geometries on pH and boron concentration. The preference of the main borate geometries, which is typically trigonal for the heavier and tetrahedral for the lighter boron isotopes, also contributes to this phenomenon [29–38]. The so-called durability of the final waste forms is one of the most important quality parameters of the long-term waste disposals performance assessment analysis [4, 12, 39–43].

This study aims to provide better understanding and compare the behavior of NBA and EBA in cementitious structures, as they are the most common hosting matrix for low and intermediate radioactive wastes. The simplest and the most common cement type, ordinary Portland cement (OPC) was used for the experiments. The assessments were focused on leaching tests, in which boron leachability has been selected to be the main parameter to describe the chemical stability of simulated waste forms.

Experimental

For the purposes of this study the following experimental stages were followed: simulation and investigation of NBA- and EBA-liquid radioactive wastes, cementation of the liquid wastes and preparation of solid specimens (simulated final waste forms), mineralogical analysis of hardened cement pastes before leaching, leaching tests, analysis of leachates and, mineralogical analysis of hardened cement pastes after leaching.

Preparation and characterization of simulated liquid boric acid wastes

Simulated wastes with boron concentrations and enrichments specified in Table 1 were prepared at Centre for Energy Research, Hungary. The boron concentration covered a range of 20–60 g/l, which is the average boron concentration of residues in NPP evaporated sludge [3, 4, 20, 44–48]. EBA powder ($^{10}B > 95\%$) and crystalized ortho-boric acid powder with natural isotopic abundance ($^{10}B = 19.9\%$) were used. Both types of boric acid powders were mixed with demineralized (DM) water (conductivity = 1.1 μS/cm, pH = 7.5 at 23 °C) in the synthesis of the simulated EBA and NBA waste solutions.

To increase the boric acid solubility in DM water, having completely homogeneous mixtures, and to decrease the cement retarding effect of boron, the simulated waste solutions were neutralized by adding granular sodium hydroxide with 1.25 of $NaOH/H_3BO_3$ molar ratio. This ratio was an optimum determined by preliminary tests with 0 to 2.5

Table 1 Specifications of simulated liquid boric acid wastes used for preparing cement pastes

Sample ID	Boron elemental concentration (g/l)	^{10}B enrichment (%)
LE2 *	20	95
LN2**	20	19.9
LE4	40	95
LN4	40	19.9
LE6	60	95
LN6	60	19.9

*LE: Liquid waste containing EBA

**LN: Liquid waste containing NBA

ratios, which provided the highest alkalinity before the start of any polymerization or crystallization process [4, 6, 21, 34, 45, 49–52]. The pH results of this step were benchmarked by geochemical modeling (PHREEQC ver.3, PHREEQC.DAT).

The prepared solutions (Table 1) were analyzed with Raman spectroscopy to clarify the effect of boron isotopic enrichment and concentration on the molecular properties of the simulated liquid wastes. These specifications help understanding the interaction of the solutions with cement clinkers during cement hydration. Raman spectroscopy was carried out on solutions poured into 10 ml volume ceramic sample holder using a HORIBA JobinYvon LabRAM HR 800 Raman micro-spectrometer. A frequency-doubled Nd-YAG green laser with a 532 nm excitation wavelength was used to illuminate the samples, displaying 130 mW at the source and ~50 mW at the sample surface. OLYMPUS 50× (numerical aperture—N.A. = 0.6) and 100× (N.A. = 0.9) objectives were used to focus the laser. A 200 μm confocal hole, 600 grooves/mm optical grating, and 30 s cumulated exposition time were used with 3 accumulations. The spectral resolution of measurements was 3.0 cm^{-1}. Raw spectra were evaluated, including baseline correction and peak fitting using Gaussian–Lorentzian functions with the LabSpec v5.5 software. The contribution of the ceramic sample holder on the Raman spectra was excluded based on blank measurements of the holder with the same acquisition settings. The measurements were repeated at least five times to reach the uncertainties of the results.

Preparation of simulated waste forms

Cement characterization

Ordinary Portland cement (OPC, CEM I-52,5N), the most common and simplest type of cement, with the given chemical and mineral compositions (Table 2) was mixed with the simulated liquid boric acid wastes (Table 1) and with pure DM water as the reference to prepare cement pastes

Table 2 Chemical and mineralogical specifications of the Portland cement used for preparing the cement pastes, the data is provided by CEM-KUT Ltd

Chemical compositions of major elements									
Oxides	SiO_2	Al_2O_3	Fe_2O_3	CaO	MgO	K_2O	Na_2O	SO_3	Cl^-
(m/m %)	19.71	5.3	3.75	65.03	2.41	0.33	0.43	3.03	0.016
Phase composition									
Name	Alite (C_3S)	Belite (C_2S)	Tricalcium aluminate (C_3A)	Tetracalcium aluminoferrite (C_4AF)	Calcium sulfate				
Chemical formula	Ca_3SiO_5	Ca_2SiO_4	$Ca_3Al_2O_6$	$Ca_4Al_2Fe_2O_{10}$	$CaSO_4$				
Weight percentage (m/m %)	60.94	10.95	7.7	11.41	5.22				

(Table S1). The applied water-to-cement mass ratio (W/C) was adjusted to 0.4 [4, 12, 21, 39, 40, 45, 53, 54]. The resulting cement pastes have about 2.4–6.8% cement content for the 20–60 g/l boron in liquid wastes, respectively, while the usual mass ratio for the used cement is between 10 and 12% [20, 21].

Mixing, casting and curing

The cement powder was first poured into a mixer (HAUSER DM-601), and then the simulated liquid boric acid waste was added to the cement step by step. The mixture was stirred mechanically (90 rpm for 12 min) at the normal lab conditions (T = 23 °C, RH = 70%) to obtain a completely homogeneous paste [51]. The wet paste was filled into 2.5 cm diameter and 5 cm height Polyethylene cylindrical molds [55]. The molds were then shaken for 5 min to remove air bubbles from the paste [56]. Then, the molds were put in an incubator (VWR-INCU Line 68R) with a fixed temperature of 20 ± 0,1 °C [55]. The specimens were cured for 28 days, and then they were de-molded by a manual-hydraulic press (SPECAC 25 T) [44, 57]

Leaching tests

Leaching tests followed the procedure described in ASTM C1308-21 standard [55]. The cylindrical solid samples with 50 cm² contact surface were immersed in 500 ml DM water (leachant), and the resulting solutions (leachates) were changed and sampled in time intervals of 2, 5, 17, and 24 h and then daily for the next 10 days (Figure S1).

Chemical analysis of the leachates

The pH values of the leachates were measured by calibrated pH meter (Mettler Toledo SevenExcellence). The changes in pH can signify different chemical compounds released

into the leachates [39, 40, 58–60]. Each leachate was filtered through a cellulose acetate membrane (pore diameter of 0.45 μm) and acidified with ultrapure nitric acid. The solutions were analyzed for the total released boron and its isotopic ratio ($^{10}B/^{11}B$) by inductively coupled plasma optical emission spectrometry (ICP-OES; Perkin Elmer Avio 200) and inductively coupled plasma mass spectrometry (ICP-MS; Thermo Finnigan-Element2), respectively [61].

Chemical and phase analysis of the cementitious specimens

To evaluate the effects of applying different simulated liquid wastes with different concentrations and enrichments and to understand the results of leaching phenomenon on the solidified specimens, morphological, elemental, and mineralogical analyses were carried out on all the cylindrical solid specimens before and after the leaching test. The cylindrical samples were cut in half and after dry polishing of the cut surface (BUEHLER silicon carbide paper; Grit 500) scanning electron microscopy and energy dispersive X-ray spectroscopy (SEM–EDX; Thermo Scientific, Scios 2) measurements were performed. In addition, 3 g of the exterior rims (affected area) of all the leached and untreated solidified specimens were sampled by a drill, powdered, sieved (63 μm), and analyzed with X-ray diffraction (XRD; Bruker D2 Phaser diffractometer).

Calculation methods

Incremental fraction leached (IFL) Based on the standard procedure, the unitless incremental fraction leached (IFL_n) of boron during the nth test interval is calculated using Eq. (1):

$$IFL_n = a_n^B / A_0^B \tag{1}$$

where a_n^B (mg/l) is the quantity of boron measured in the leachate from the nth test interval, and A_0^B (mg/kg) is the quantity of boron in the solidified specimen at the beginning of the test (Table S1).

Cumulative fraction leached (CFL) The cumulative fraction leached (CFL$_j$) of boron until the jth interval is calculated by Eq. (2):

$$CFL_j = \sum_{n=1}^{j} a_n^B / A_0^B = \sum_{n=1}^{j} IFL_n \qquad (2)$$

Plotting the CFL values versus the cumulative time provides a straightforward graphical comparison of leaching data from the various solidified cementitious samples [55]. These results can be later used in modeling calculations to predict the long-term leaching behavior and the overall durability and performance of final waste forms [62].

Results and discussion

Adjustment of pH for the simulated liquid boric acid wastes

The effect of changing the NaOH/H$_3$BO$_3$ molar ratio on pH of the simulated wastes (both EBA- and NBA-solutions) are shown for experimental and modeling results (Fig. 1). The measured pH curves of EBA and NBA solutions overlap well with each other and with the modeled pH by PHREEQC. Accordingly, there is a generally positive relationship between pH and NaOH/H$_3$BO$_3$ ratios of 0–1.25, but both methods show no notable pH changes between 1.25–1.5 ratio. On the other hand, during the experiments, the NBA and EBA solutions with NaOH/H$_3$BO$_3$ ratios above 1.5 got
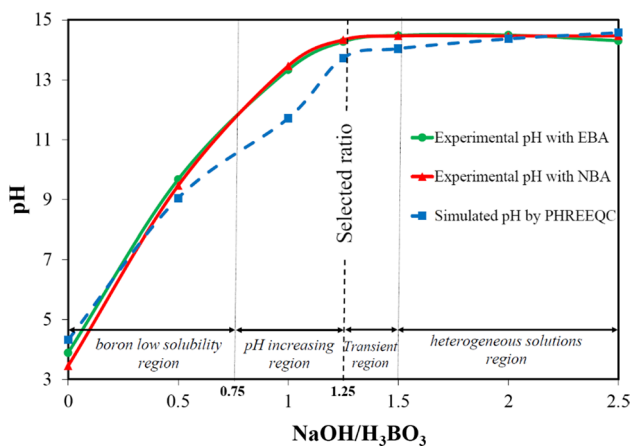

Fig. 1 Measured and modeled effect of changing the NaOH/H$_3$BO$_3$ ratio on the pH of the simulated liquid boric acid wastes

polymerized and crystallized, respectively and became heterogeneous, which should be avoided [52][63]. Therefore, during the preparation of simulated liquid boric acid wastes, the NaOH/H$_3$BO$_3$ ratio was adjusted to 1.25 to reach the highest possible pH (the longest possible durability for cementitious matrices) but keeping homogeneity [63].

Results of Raman spectroscopy measurements of simulated liquid wastes

The Raman spectra of the concentrated liquid boric acid wastes (Table 1) are illustrated in Fig. 2 for the optimal zone of the characteristic Raman bands of borate solution investigations, 400–1700 cm^{-1} [64–70]. For all the samples, four characteristic Raman bands appeared on the spectra (Fig. 2). Two bands are at 521 and 745 cm^{-1} which can be identified as for B$_5$O$_6$(OH)$_4^-$ and B(OH)$_4^-$ molecules, respectively [64, 65]. The other detected bands are at 1646 cm^{-1} which relates to water [71–73]. Bands at 930 cm^{-1} (NBA solutions) or 960 cm^{-1}(EBA solutions) also show up, possibly related to B–O bands in complicated heavy molecules containing boron and sodium atoms [74, 75]. However, their identification is not established yet. The results of intensity and integrated bands area of the different bands (S$_p$) are summarised in Table 3.

For both NBA and EBA solutions, the S$_p$ of the bands at 521, 745, and 930/960 cm^{-1} increase together with boron concentration, whereas the band of water at 1646 cm^{-1} decreases with increasing boron concentration (Fig. 2 and Table 3). Additionally, for the known bands of borate molecules at 521 cm^{-1} (B$_5$O$_6$(OH)$_4^-$) and 745 cm^{-1} (B(OH)$_4^-$), the ratio of their integrated areas (RS$_p$, Eq. 3), and the relative comparison of RS$_p$ between NBA and EBA at a fixed concentration ($\Delta RS_{P(EBA/NBA)}$, Eq. 4) are summarised in Table 3. These two provide us the comparability e the molecular ratio of $B_5O_6(OH)_4^-$ and $B(OH)_4^-$ in the studied liquid wastes (Table 3).

$$RS_p = S_{p_{745(B(OH)_4^-)}} / S_{p_{521\left(B_5O_6(OH)_4^-\right)}} \qquad (3)$$

$$\Delta RS_{P(EBA/NBA)} = \left(RS_{P(EBA)} - RS_{P(NBA)} \right) / RS_{P(EBA)} \times 100 \, [\%] \qquad (4)$$

where $S_{p_{745(B(OH)_4^-)}}$ and $S_{p_{521(B_5O_6(OH)_4^-)}}$ are the integrated areas under the specific bands for B(OH)$_4^-$ and B$_5$O$_6$(OH)$_4^-$, and $RS_{P(EBA)}$ and $RS_{P_{EBA}}$ are the ratios of the integrated areas of these two bands at EBA and NBA solutions, respectively.

For each boron concentration, the RS$_p$ of the enriched sample ($RS_{P(EBA)}$) is bigger than that of the natural sample ($RS_{P(NBA)}$), and the percentage of this difference ($\Delta RS_{P(EBA/NBA)}$) is decreasing from 26.9 to 4.7% with increasing the boron concentration in the solution from 20 to 60 g/l (Table 3).

521 cm^{-1} → B$_5$O$_6$(OH)$_4^-$; 745 cm^{-1} → B(OH)$_4^-$; 1446 cm^{-1}→H$_2$O; 930/960 cm^{-1} → B-O bonds in complicated heavy sodium-borate molecules
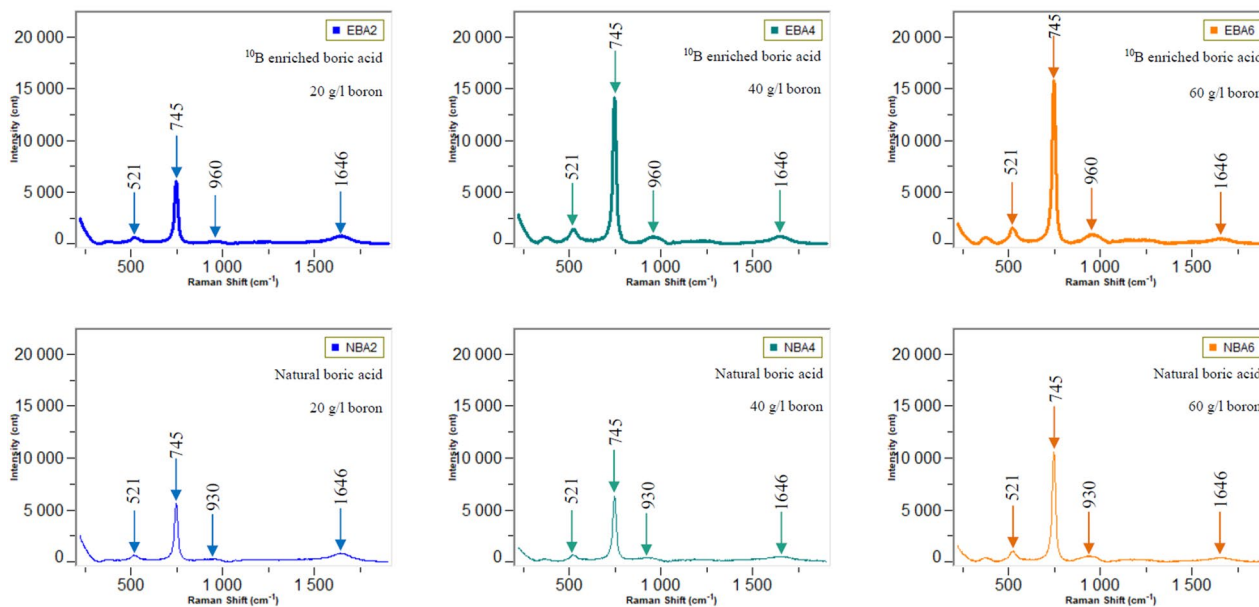

Fig. 2 Raman spectra of the simulated liquid wastes containing different enrichments and concentrations of boric acid (NBA: natural boric acid; EBA: ^{10}B enriched boric acid; 2, 4, and 6 represent 20, 40, and 60 g/l boron in the simulated liquid wastes)

$$S_p RS_p S_{p_{745(B(OH)_4^-)}} S_{p_{521\left(B_5O_6(OH)_4^-\right)}} \Delta RS_{p_{(EBA/NBA)}} RS_{P_{(EBA)}} RS_{P_{(NBA)}} RS_{P_{EBA}}$$

Results of XRD analysis of solid samples

The semiquantitative XRD results of all the cementitious solid samples before and after the leaching tests are summarized in Table 4, XRD patterns used for phase identification are presented in Figure S2. For both leached and untreated samples and for both boron enrichments (NBA, 19.9% and EBA, 95% ^{10}B), as the initial concentration of boric acid increases, the hydration level of cement decreases, subsequently the amount of the cement hydration products (ettringite) significantly increases (Table 4). At each fixed concentration, the solid specimens made with EBA show a higher level of hydration than the specimens made with NBA (Table 4). As the effect of boric acid addition to the cement pastes, the formation of minerals containing boron such as gowerite [CaB$_6$O$_{10}$·5H$_2$O] and biringuccite [Na$_2$B$_5$O$_8$(OH)$_2$)·H$_2$O], were recorded (Table 4).

XRD results also indicate that during the leaching test, all the boron-bearing minerals (i.e., gowerite and biringuccite) have disappeared (dissolved) from the exposed external rim of the NBA specimens, whereas there are some remaining boron-containing phases (biringuccite) at the rim of the specimens made with the highest concentration of EBA (Table 4). Also, a small amount of boron-containing mineral,

called meyerhofferite [Ca$_2$B$_6$O$_6$(OH)$_{10}$·2(H$_2$O)] was detected in the specimens before the leaching test that during the experiment have decreased (dissolved) from the exposed external rim of both the NBA and EBA samples (Table 4).

Results of SEM analysis of the solidified cementitious materials

The backscattered-electron (BSE) images of SEM measurements of the solid cement paste samples were analysed before leaching (SE4, SE6, SN4, SN6 and Reference samples) and after leaching (LSE4, LSE6, LSN4 and LSN6) using ImageJ software [76], which is a versatile, open-source used for a variety of tasks, such as simple image enhancements and quantitative image analysis. (Users can perform statistical analysis, extract quantitative data from photographs, and visually explore and edit digital images.) The threshold brightness histogram analysis method algorithm option in the ImageJ software was applied to perform area analysis by highlighting the brightness levels on the surface of the samples to infer and quantify the lighter unhydrated clinker phases from darker hydrated matrix phases (in the Supplementary Materials, Fig S3, which is the original mosaic picture).

The results of the analyses quantified the unhydrated surface areas of the samples before leaching as SE4 (239,493.731 µm^2), SE6 (248,245.86 µm^2), SN4 (238,675.265 µm^2), SN6 (326,395.155 µm^2), reference

Table 3 Summary of the Raman spectroscopy analysis on EBA- and NBA-liquid wastes

Band (cm^{-1})	Intensity (count)	$S_p \pm$ error% (cm^2)	$RS_{p(EBA)}$	Band (cm^{-1})	Intensity (count)	$S_p \pm$ error% (cm^2)	$RS_{p(NBA)}$	$\Delta RS_{p(EBA/NBA)}$ (%)
LE2				LN2				
521.2	599	24,798 ± 3.1	3.8	521	615	32,084 ± 4.7	2.8	26.9
745.8	6037	94,899 ± 0.5		745.8	5592	89,809 ± 0.51		
960.9	265	16,930 ± 2.5		930.7	283	29,274 ± 3.7		
1646.0	765	73,206 ± 3.7		1645.1	835	86,118 ± 3.6		
LE4				LN4				
521.2	1397	54,810 ± 2.9	4.2	520.9	675	34,088 ± 4.5	3.6	14.4
746.0	14,057	231,782 ± 0.7		745.6	6188	123,396 ± 1.6		
960.1	660	49,072 ± 2.2		930.8	385	45,051 ± 2.9		
1646.8	684	73,045 ± 5.5		1646.5	521	84,026 ± 4.6		
LE6				LN6				
521.7	1519	61,389 ± 2.8	4.8	521.7	1027	43,996 ± 3.9	4.6	4.7
745.8	15,865	294,041 ± 0.3		745.7	10,551	200,747 ± 0.7		
960.0	881	67,460 ± 4.9		930.9	525	48,160 ± 4.1		
1646.7	469	56,574 ± 4.2		1646.9	420	47,781 ± 5.4		

LE: liquid waste containing 95% ^{10}B enriched boric acid; LN: liquid waste containing natural boric acid; 2, 4, and 6 represent 20, 40, and 60 g/l boron in liquid waste; S_p: integrated area under band; $RS_p = S_{p_{745(B(OH)_4^-)}}/S_{p_{521(B_5O_6(OH)_4^-)}}$; $\Delta RS_{p(EBA/NBA)} = (RS_{P_{(EBA)}} - RS_{P_{(NBA)}})/RS_{P_{EBA}} \times 100$ [%]

(53,714.927 μm^2); whereas samples after leaching as LSE4 (246,095.847 μm^2), LSE6 (239,826.99 μm^2), LSN4 (316,751.896 μm^2) and LSN6 (474,797.571 μm^2) using uniform surface area for the statistical analyses. These results seem to indicate a positive correlation between increasing boric acid concentration from 0 g/l in the reference, samples to 60 g/l in SE6 and SN6 showing an increasing surface area of unhydrated clinker phases of 272,680.228 μm^2 observed on the samples (Fig. 3) implying the possibility of increased hydration retardation with increasing boric acid concentration. It is also observed from this results that natural boric acid (samples LN4 and LN6) shows a higher retarding on the OPC hydration process than the enriched boric acid (samples SE4 and SE6). The result also indicates that both types of boric acids (either enriched or natural one) show significant hydration retardation effect in comparison with the reference sample (Fig. 3).

Also, the SEM data are in good agreement with XRD results (Table 4) as boric acid concentration increases so does the amount of unreacted clinker phases observed on the sample surface (Ref. to the original mosaic picture which is supposed to be in Suppl. Mat. as suggested above) and a decrease of the secondary hydration phase production (like ettringite) observed in the XRD results (Table 4). Furthermore, the BSE images show that the leachant (DM water) effect the solidified specimens (compared to the reference sample), and an alteration layer of 300 μm appeared after the leaching period of 11 days (Fig. S4).

Results of leachates analysis

pH measurements

The measured pH for all the leachates shows similar and generally decreasing trends for all the samples (Figure S5). All the pH results are between 11.5 and 12.3. A notable pH variation ($|\Delta pH| < 0.5$) during the first 2 days was recorded, which is mostly due to the inequality of the sampling intervals (Figure S5).

Table 4 Semiquantitative XRD results of the cementitious samples before and after the leaching tests

	SE2	SN2	SE4	SN4	SE6	SN6	Ref*
Cementitious samples before leaching (m/m %)							
Alite	42	50	52	46	58	60	34
Belite	4	11	–	–	–	–	4
Portlandite	26	19	19	18	14	14	39
Ettringite	3	2	–	–	–	–	5
Akermanite	2	1	3	4	4	4	2
Brownmillerite	3	3	2	3	2	3	4
Hydrocalumite	4	3	7	8	7	4	3
Kanemite	–	–	2	6	1	1	–
Biringuccite	8	3	5	6	4	5	–
Gowerite	–	–	1	2	4	4	–
Meyerhofferite	–	–	–	–	–	–	–
Amorph	8	8	9	7	6	5	9

	LSE2	LSN2	LSE4	LSN4	LSE6	LSN6
Cementitious samples after leaching (m/m %)						
Alite	50	56	70	72	69	70
Belite	8	4	–	–	–	–
Portlandite	22	18	12	10	9	11
Ettringite	3	2	–	1	–	–
Akermanite	–	1	1	1	1	1
Brownmillerite	5	5	4	3	3	2
Hydrocalumite	4	4	4	4	4	3
Kanemite	–	–	–	–	–	–
Biringuccite	–	–	–	–	3	–
Gowerite	–	–	–	–	–	–
Meyerhofferite	–	–	–	–	3	3
Amorph	8	10	9	9	8	10

*Ref: boron concentration is zero in the reference sample; SE: solidified sample with enriched boric acid (95% ^{10}B) before leaching; SN: solidified sample with natural boric acid (19.9% ^{10}B) before leaching; LSE: leached solid sample containing enriched boric acid (95% ^{10}B); LSN: leached solid sample containing natural boric acid (19.8% ^{10}B); Numbers of 2, 4 and 6 represent 20, 40, and 60 g/l boron in the simulated liquid wastes

Elemental boron release measurements

The concentrations of leached boron (a^B) during each time interval of the leaching test are summarized in Table S2-S4. For all the tests, there was a high peak of boron release at the third interval (17 h). The results of Table S2-S4 were used to calculate the percentage of leached boron (($\sum^{11\text{day}} a^B$)/A_0) from all the solidified specimens (Fig. 4). Accordingly, during the leaching period (11 days), the percentage of released boron from all the solidified samples is between 0.62 and 1.12 m/m %. Furthermore, Fig. 4 shows an obvious increase in boron leaching for both EBA and NBA specimens with the growth of the initial boron concentration in the samples. However, at each initial boron concentration, the specimen made with NBA shows a higher percentage of leached boron than that made with EBA (Fig. 4).

The CFL value of boron, calculated using data in Table S2-S4 and following Eqs. (1–2), is plotted versus time in Fig. 5. According to these curves, (1) the CFL grows with the initial boron concentration in the samples (20, 40, and 60 g/l boron), and (2) at each fixed boron concentration, the cementitious specimen made with EBA shows lower CFL than that of made with NBA. The differences between EBA and NBA's CFL values are getting more significant from 3 up to 29% as the boron concentration in the liquid wastes increases from 20 to 60 g/l.

In addition, to get a better understanding of boron leaching kinetics, a new parameter, the rate of leaching (R_n), is introduced by Eq. (5), which is a modified formula of Sun et al. [46]:
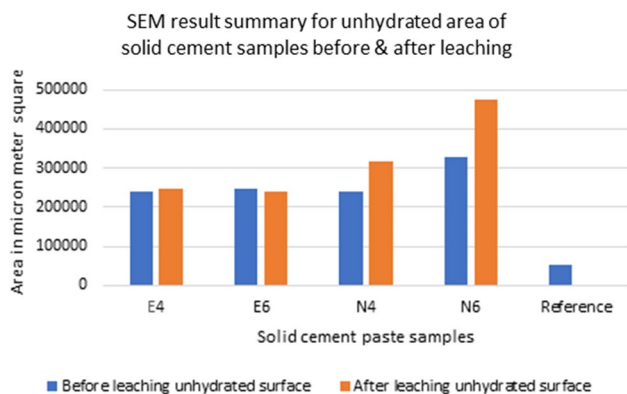
Fig. 3 Summary of SEM analysis of the cementitious specimens before and after the leaching tests using the ImageJ software threshold brightness histogram analysis method algorithm to quantify unhydrated areas: E4 with enriched boric acid of 40 g/l concentration; E6 with enriched boric acid of 60 g/l concentration; N4 natural boric acid of at 40 g/l concentration; N6 natural boric acid of 60 g/l concentration, whereas the reference sample was made with OPC and DM water
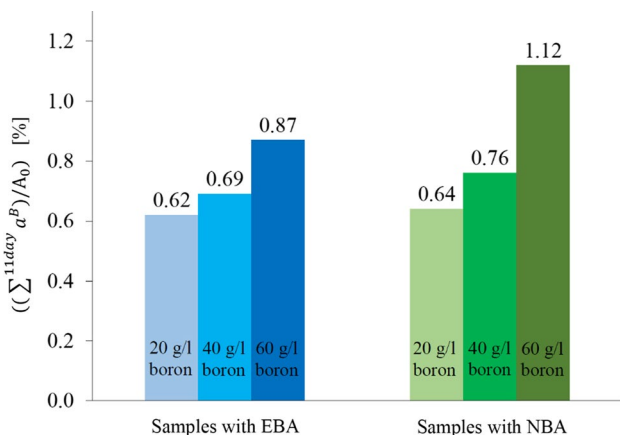

Fig. 4 Percentage of leached boron in contrary to changing boron concentration and enrichment ($\sum CFL_B$: cumulative leached boron at the end (11 days) of leaching test; EBA: 95%. ^{10}B enriched boric acid; NBA: natural boric acid; A_0 = initial boron concentration in the cement pastes)

$$R_n = \frac{IFL_n}{(D_n \times S/V)} \; [cm/s] \qquad (5)$$

where R_n is the rate of boron leaching, D_n is the duration of the nth time interval (s), S is the surface area (m^2), and V is the volume of the solidified specimens (m^3). The results of R_n show the net amount of leaching rate independent of the duration of each test interval (Fig. 6).

As shown in Fig. 6, at the beginning of the leaching test (2 h), all the samples show the highest rate of leaching. This is followed by a short drop in the values (5 h) and then again, an increase (17 h). After these changes, all the curves show
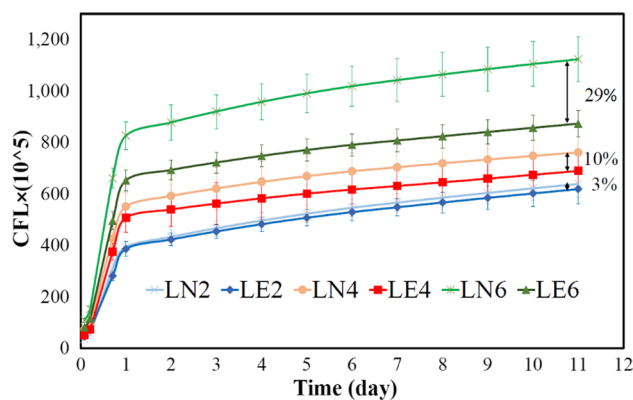
Fig. 5 Cumulative fraction leached (CFL, Eq. 2) of boron versus time (CFL: cumulative fraction of leached boron; LE: leachate from solidified specimens containing 95% ^{10}B enriched boric acid; LN: leachate from solidified specimens containing natural boric acid; 2, 4, and 6 represent 20, 40, and 60 g/l boron in the simulated liquid wastes)
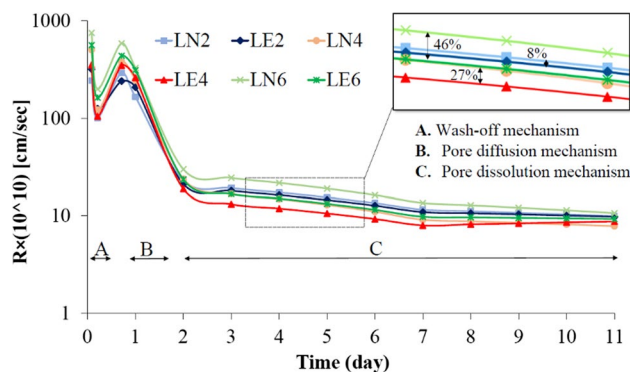
Fig. 6 Logarithmic rate of boron leaching (R$_n$, Eq. 5) versus time (R: rate of leaching; LE: leachate from solidified specimens containing 95% ^{10}B enriched boric acid; LN: leachate from solidified specimens containing natural boric acid; 2, 4, and 6 represent 20, 40, and 60 g/l boron in the simulated liquid wastes) [56]

a continuous decrease in the leaching rate (Fig. 6). As a comparison among the cementitious specimens with different boron concentrations and enrichments, the rate of boron leaching (R$_n$) increased with the initial boron concentration in the samples and is lower for specimens made with EBA than the specimens with NBA (Figs. 6). These R$_n$ differences between EBA and NBA specimens are increased one order of magnitude as the boron concentration in the liquid wastes increases from 20 to 60 g/l.

Isotopic distribution of leached boron

The ICP-MS results of boron isotopic distributions in the leachates of EBA and NBA simulated waste forms are plotted in Figs. 7 and 8, respectively. For the EBA-specimens the ^{10}B/^{11}B ratios in the leachates show a significant decreasing
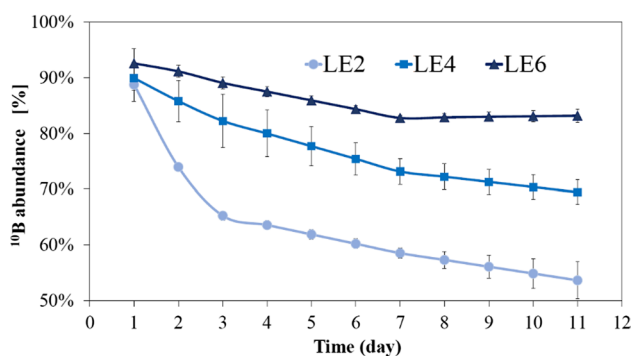
Fig. 7 Isotopic leachability of boron from the solidified specimens containing 95% ^{10}B enriched boric acid (EBA) (LE: leachate from the specimens containing 95% ^{10}B enriched boric acid; 2, 4, and 6 represent 20, 40, and 60 g/l boron in the simulated liquid wastes)
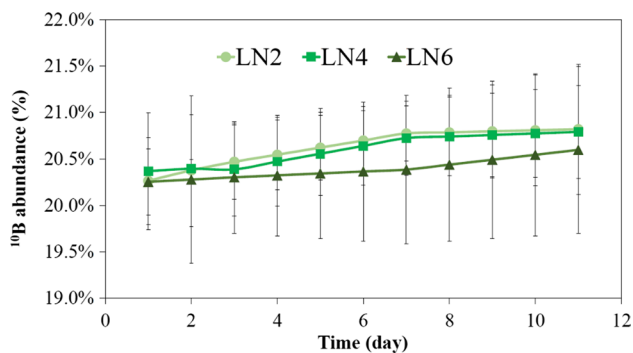

Fig. 8 Isotopic leachability of boron from the solidified specimens containing natural boric acid (NBA). (LN: leachate from the specimens containing natural boric acid; 2, 4, and 6 represent 20, 40, and 60 g/l boron in the simulated liquid wastes)

trend during the 11 days of the leaching test (Fig. 7). In the beginning of the leaching experiments boron dissolves from the surface and diffuses from the near-surface regime of the samples. The measured ^{10}B abundance (around 90%) is close to the initial one (95%). As the experiment proceeds the boron built-in in the inner part of the sample starts to leach and the ^{10}B abundance decreases suggesting different diffusion coefficient and leachability of the isotopes. [35, 38, 77, 78].

For the samples from the leaching tests of the NBA-specimens, the ^{10}B/^{11}B ratio showed no significant variation during the test period (Fig. 8). The minor changes were lower than the uncertainty of the measurement technique.

Discussion

Chemical and geometrical characterizations of EBA- and NBA-liquid wastes

Since the boron concentration in the studied solutions (20–60 g/l or ~ 2–6 M boron) is higher than the concentration level where only monoborates are expected (0.2 g/l or 0.025 M boron) [31, 52, 64, 65, 67, 70, 79, 80], all the boron in the studied liquid wastes tends to occur in heavy polyborate molecules ($B_x(OH)_{3x+y}^{y-}$, x > 6, and 0 < y < 3). However, polymerized solutions would create heterogeneous liquid wastes what cannot be effectively immobilized by cementitious materials [51]. To overcome this unfavorable phenomenon (polymerization of the highly concentrated boric acid wastes), the NaOH addition was optimized ($NaOH/H_3BO_3 = 1.25$, Fig. 1), and hence, only moderate-size polyborates ($B_x(OH)_{3x+y}^{y-}$, 3 < x < 6 and 0 < y < 3) including $B_3O_3(OH)_4^-$, $B_4O_5(OH)_4^{2-}$, and $B_5O_6(OH)_4^-$ are expected [64, 65]. Meanwhile, the formation possibility of these polyborates is not the same, because at the very high alkalinity (pH > 11), the OH^- ions attack the BO_3 bonds in polyborates, depolymerize them and cause to forming $B(OH)_4^-$ ions alternatively [64, 67]. The results of Raman spectroscopy analysis on the studied simulated liquid wastes are in general agreement with previous knowledge from the literature [64–67, 80], where, for the simulated liquid wastes, the main significant borate forms are mono tetrahedral borate ($B(OH)_4^-$ with the specific band at 745 cm^{-1}) and poly pentaborate ($B_5O_6(OH)_4^-$ with the specific band at 521 cm^{-1}) (Fig. 2).

Furthermore, the results of Raman analysis (Table 3) show that at each boron concentration, the ratio of the integrated area under the main bands ($RSp = S_{B(OH)_4^-}/S_{B_5O_6(OH)_4^-}$) of the EBA solutions is bigger than that of the NBA solution up to 26.9%. This indicates that at each boron concentration, the possibility of $B(OH)_4^-$ formation in the EBA-liquid waste is higher than that of the NBA-liquid waste. This difference is due to the molecular structure and isotopic preference of $B(OH)_4^-$ and $B_5O_6(OH)_4^-$ in EBA and NBA liquid wastes (Fig. 9). The molecular structure of $B_5O_6(OH)_4^-$ consists of four trigonal and one tetrahedral borate positions, whereas $B(OH)_4^-$ composed of only one tetrahedral borate position (Fig. 9). According to previous knowledge [38, 79, 81–83], the trigonal borate geometry is more stable with the heavier boron isotope (^{11}B), whereas the tetrahedral borate geometry prefers the lighter boron isotope (^{10}B). Therefore, resulting in these geometric compositions and isotopic preferences of the borates, the possibility of $B(OH)_4^-$ formation is higher in EBA liquid waste than in NBA liquid waste.

The intensity of the band specific to water (1646 cm^{-1}) decreases with increasing boron concentration (Fig. 2 and
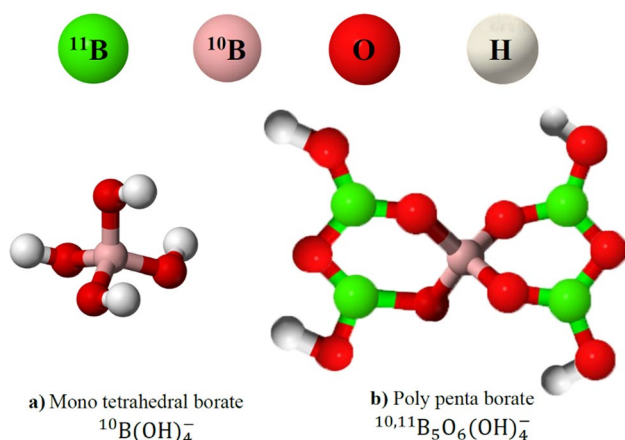
Fig. 9 Molecular structure and isotopic preferences of a) $B(OH)_4^-$ and b) $B_5O_6(OH)_4^-$. $B(OH)_4^-$ consists of one tetrahedral position, which favors ^{10}B and $B_5O_6(OH)_4^-$ consists of one tetrahedral and four trigonal positions, which mostly prefers ^{11}B

Table 3). This is due to the decrease in the water-mass ratio in the solutions with increasing the boron concentration from 20 to 60 g/l cm^{-1}.

The solid samples mineralogy versus the initial boron concentration and enrichment

The influence of changing boric acid concentration on the mineralogy of the cementitious specimens (Table 4 and Fig. 3) is mostly related to the boron retarding effect on cement hydration [45, 58, 84–86]. The decreasing level of hydration can leave more unreacted clinkers in the cement pastes (Table 4). These remaining clinkers can adversely affect the physical properties of the cement paste, including porosity and compressive strength, and subsequently, the durability of the simulated final waste forms decreases [11, 84, 87, 88]. Furthermore, the formation of ettringite, which has a significant potential for building boron atoms into its structure [4, 9, 13, 14], is detected only in the samples with low boron concentration (Table 4). Therefore, since the increase in boron concentration reduces the cement hydration and also the formation of ettringite, the maximum initial boron concentration in the cementitious matrices (maximum solid loading on cement) should be optimized for both NBA and EBA solidified specimens [20, 21].

The differences in the mineralogy of the solidified specimens with applying NBA or EBA (Table 4) are mostly related to the molecular differences of the simulated liquid boric acid wastes before mixing with cement ("Chemical and geometrical characterizations of EBA- and NBA-liquid wastes"). Since the liquid wastes containing different types of boric acid enrichments (NBA and EBA) can create varied ratios of the distinct forms and geometries of boron-molecules (Figs. 10a and c), these molecules can cause different chemical interactions with the cement clinkers and consequently, variable mineralogy's can be formed during the cement and liquid wastes mixing (Table 4).

Solid samples mineralogy versus running leaching tests

In accordance with previous studies [42, 60, 89–91], the results of our experiments showed that water diffuses from the surface into the interior parts of the cementitious matrices during the leaching test (Fig. 3h). Due to the high natural boron-salt solubility [92], all the boron-bearing minerals (i.e., biringuccite and gowerite) get released from the NBA-specimens. However, only some of those minerals from the EBA-specimens are released from the affected depth of the solidified matrix (data of Table 4 for before and after the leaching test), which is due to the higher stability of borate molecules in EBA solidified specimens as discussed above ("Boron leachability versus boron enrichment"). During dissolution, the more boron-containing minerals are released from the cementitious structure (NBA-cementitious specimens in this study), the higher porosity becomes, and consequently, shorter durability of the simulated final waste form made with NBA is expected compared with the specimens made with EBA [39, 40].

Boron leachability versus initial boron concentration

The positive relationship between the total leached boron and the initial boron concentration (Fig. 5) is due to the more availability and the subsequent higher possibility of boron-containing minerals getting dissolved from the cementitious host structure [93]. Nevertheless, high leachability can lead to lower chemical stability and durability for the solidified specimens, which is a critical parameter in the long-term disposal of cementitious waste. Not only the net amount of mass (CFL, Fig. 5) but also the percentage of total boron leached (Fig. 4) shows a continuous growth together with the increase of the initial boron concentration in the specimens. This phenomenon may be related to the porosity increase as the initial boron concentration grows (discussed in "Solid samples mineralogy versus running leaching tests" section) and the constraint of cementitious matrices to hold other solid materials or precipitating boron-bearing minerals from boric acid solutions [20, 58, 93].

Boron leachability versus boron enrichment

At each initial boron concentration, the solidified specimens made with EBA show lower boron leachability (both amount and rate) than those made with NBA (Figs. 4, 5, 6). This phenomenon is related to the chemical speciation
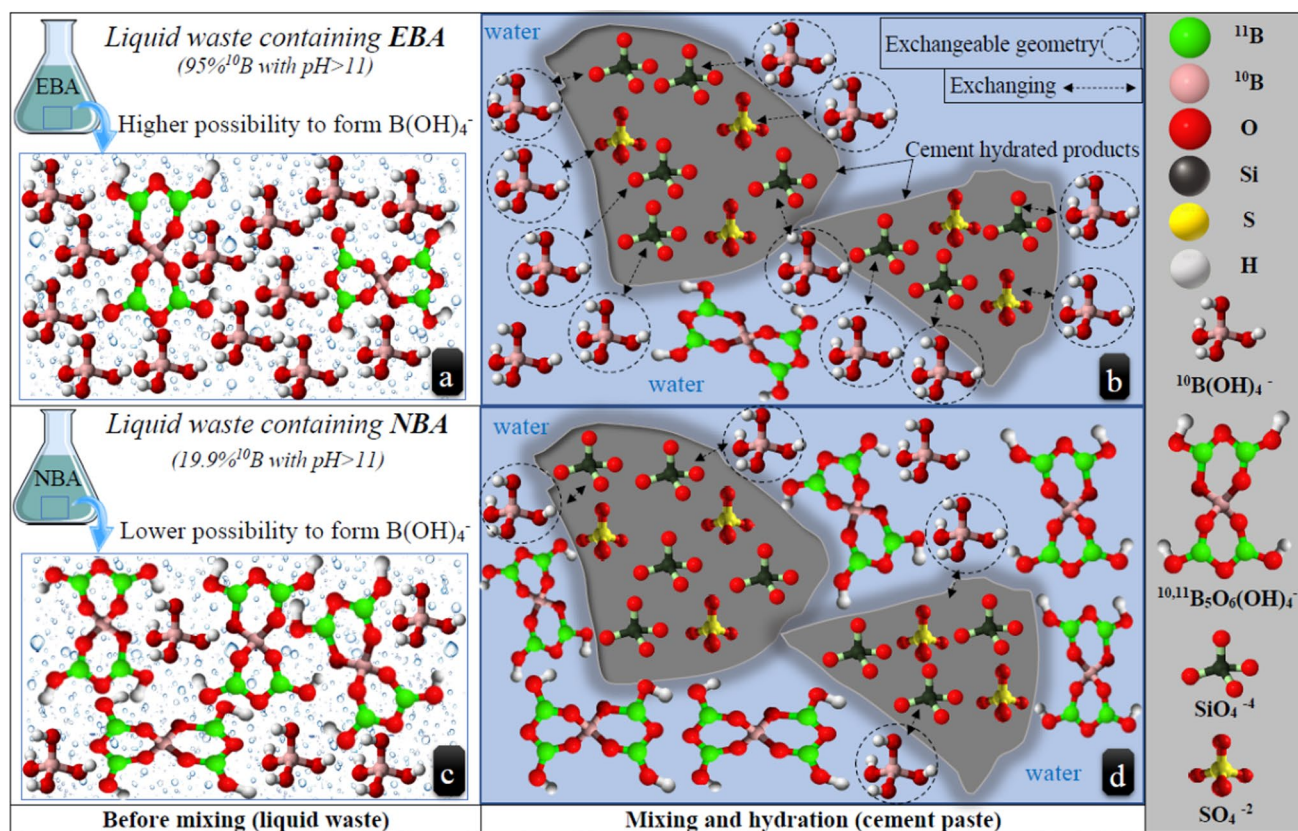
Fig. 10 Two of the most important borate molecule geometries in EBA and NBA solutions and their interaction with cement clinker: **a** liquid waste containing 95% ^{10}B enriched boric acid, EBA; **b** interaction and substitution of EBA-liquid waste with cement clinker; **c** liquid waste containing natural boric acid, NBA; **d** interaction and substitution of NBA-liquid waste with cement clinker

of boric acid introduced in "Chemical and geometrical characterizations of EBA- and NBA-liquid wastes"–"The solid samples mineralogy versus the initial boron concentration and enrichment" sections and Fig. 10. ^{10}B(OH)$_4^-$ [3, 4, 9, 13, 14, 37, 45, 81]. However, in the NBA simulated liquid wastes, the B(OH)$_4^-$/B$_5$O$_6$(OH)$_4^-$ ratio is lower than in the EBA liquid waste (Fig. 2 and Table 3). Thus, the more abundant isotope (^{11}B) has lower possibility to locate in the interchangeable tetrahedral borate coordinates of the liquid phase and subsequently has lower possibility of substituting in the above-mentioned sites of the cement paste (Fig. 10c, d). The unsubstituted ^{11}B-containing ions and molecules can release from the cementitious matrix effectively when the solidified specimens get contacted with water (Fig. 10d). These phenomena are supported by the observations in Fig. 7, where after a rapid release of boron from the specimens' surface during the first day (surface wash-off), the abundance of released ^{10}B decreases in time, whereas the total boron leaching increases continuously due to the ^{11}B release [62, 94].

Conclusion

This study is the first about the immobilization of the novel radioactive liquid waste containing enriched boric acid. The major results and conclusions are the following: (a) the simulated radioactive wastes natural boric acid (NBA) and enriched boric acid (EBA) have different molecular compositions and isotopic specifications, in which pH and boron concentration have the dominant role to constrain these variabilities; (b) variation in chemical and isotopic specifications of enriched boric acid and natural boric acid solutions causes different interactions between their boron molecules and cement clinker which provide enriched boric acid—and natural boric acid—cementitious waste forms with different mineralogy's; (c) due to the mineralogical modifications, the elemental and isotopic leachabilities of boron from the natural boric acid—and enriched boric acid—bearing specimens were different; (d) the total amount and the rate of boron leachability from

the cementitious specimens containing enriched boric acid were lower than that of the specimens containing natural boric acid up to 29% and 46%, respectively; (e) these lower values of the amounts and rates of chemical leaching may reflect to a higher long-term stability and durability of enriched boric acid simulated waste forms compared to the natural boric acid containing type which should be considered during the long-term disposal design of radioactive wastes; (f) this phenomenon can be explained by a combination of unique molecular and isotopic properties of boron in the liquid phase including the high relative mass difference of boron isotopes, the influence of pH and boron concentration on geometry of borates and isotopic preferences of those geometries.

Declarations

References

1. Pacey N, Beadle I, Heaton A, Newsome L (2011) Chemical discharges from nuclear power stations: historic releases and implications for best available techniques (BAT). Environment Agency, Bristol

2. Xu J, Zhang W (2010) The application of ^{10}B enriched boric acid in nuclear power industry. In: International conference on nuclear engineering, proceedings, ICONE, vol 3, pp 1–5. https://doi.org/10.1115/icone18-29042

3. Palomo A, Palacios M (2003) Alkali-activated cementitious materials: Alternative matrices for the immobilisation of hazardous wastes - Part I Stabilisation of boron. Cem Concr Res 33:281–288. https://doi.org/10.1016/S0008-8846(02)00963-8

4. Sun Q, Wang J (2010) Cementation of radioactive borate liquid waste produced in pressurized water reactors. Nucl Eng Des 240:3660–3664. https://doi.org/10.1016/j.nucengdes.2010.07.018

5. Abdel Rahman RO, Zin El Abidin DHA, Abou-Shady H (2014) Cesium binding and leaching from single and binary contaminant cement-bentonite matrices. Chem Eng J 245:276–287. https://doi.org/10.1016/j.cej.2014.02.033

6. Gorbunova O (2015) Cementation of liquid radioactive waste with high content of borate salts. J Radioanal Nucl Chem 304:361–370. https://doi.org/10.1007/s10967-014-3886-3

7. Süssmilch J, Lukáš G, Fabián P, Edit TB, Nehme S, Baranyi A, Kopecsko K (2022) Solidification of radioactive evaporator residues with high borate content. Concr Struct 4:23–30

8. Baranyi A, Kopecskó K, Feil F, Gric L (2021) A paksi atomerőmű hulladékainak cementbe ágyazása, és a technológiához tartozó vizsgáló laboratórium kialakítása. Vasbetonépítés 23:31–40

9. Champenois JB, Mesbah A, Cau Dit Coumes C, Ranaidin G, Leroux F, Mercier C, Revel B, Damidot D (2012) Crystal structures of Boro-AFm and sBoro-AFt phases. Cem Concr Res 42:1362–1370. https://doi.org/10.1016/j.cemconres.2012.06.003

10. Davraz M, Pehlivanoğlu HE, Kilinçarslan S, Akkurt I (2017) Determination of radiation shielding of concrete produced from Portland cement with boron additives. Acta Phys Pol A 132:702–704

11. Ojovan MI, Varlackova GA, Golubeva ZI, Burlaka ON (2011) Long-term field and laboratory leaching tests of cemented radioactive wastes. J Hazard Mater 187:296–302. https://doi.org/10.1016/j.jhazmat.2011.01.004

12. Abdel Rahman RO, Ravil ZR, Nailia RR, Michael IO (2015) Cementitious material for nuclear waste immobilization. Wiley, London

13. Hiraga Y, Shigemoto N (2010) Boron uptake behavior during ettringite synthesis in the presence of H_3BO_3 and in a suspension of ettringite in H_3BO_3. J Chem Eng Jpn 43:865–871. https://doi.org/10.1252/jcej.10we160

14. Xu X, Liu H, Bi H, Wand S, Zhao P, Huang Y, Cheng X (2021) Stability and leaching resistance performance of SAC repair and solidification materials exposed to gamma irradiation. Constr Build Mater 302:124309. https://doi.org/10.1016/j.conbuildmat.2021.124309

15. Poellmann H, St A, Kuzel H-J, Wenda R (1993) Solid solution of ettringites. Cem Concr Res 23:422–430. https://doi.org/10.1016/0008-8846(93)90107-k

16. Csetenyi LJ, Glasser FP (1992) Borate substituted ettringites. MRS Online Proc Libr 294:273–278. https://doi.org/10.1557/PROC-294-273

17. Duque-Redondo E, Yamada K, López-Arbeloa I, Manzano H (2018) Cs retention and diffusion in C–S–H at different Ca/Si ratios. ChemRxiv. 1–7 https://doi.org/10.26434/chemrxiv.6683010

18. Tits J, Fujita T, Harfouche M, Dähn R, Tsukamoto M (2014) Radionuclide uptake by calcium silicate hydrates: Case studies with Th (IV) and U (VI) Nuclear Energy and Safety Research Department. Villigen PSI, Switzerland

19. Duque-Redondo E, Yamada K, Dolado JS, Manzano H (2021) Microscopic mechanism of radionuclide Cs retention in Al containing C–S–H nanopores. Comput Mater Sci 190:110312. https://doi.org/10.1016/j.commatsci.2021.110312

20. IAEA-TECDOC-911 (1996) Processing of nuclear power plant waste streams containing boric acid. IAEA, Vienna, Austria

21. Rakhimova NR, Rakhimov RZ, Morozov VP, Potapova LI, Osin YN (2017) Mechanism of solidification of simulated borate liquid wastes with sodium silicate activated slag cements. J Clean Prod 149:60–69. https://doi.org/10.1016/j.jclepro.2017.02.066

22. Mughabghab S, Garber D (1973) Neutron cross sections, resonance parameters. New York

23. Deruytter A, Debus G, Lauer K, Moret H, Prosdocimi A (1962) Measurement of the thermal neutron absorption cross section of boron by means of a time of flight technique. Brussels (Belgium)

24. Impink AJ, Battaglia JA, FasnachtKonopka JW, Konopka GG (1993) Enriched B-10 boric acid control system for a nuclear reactor plant (USA Patent)

25. Hongwei Z, Xuehua Z, Baoan Z (2014) Synthesis of enriched 10B boric acid of nuclear grade. Trans Tianjin Univ 20:458–462. https://doi.org/10.1007/s12209-014-2303-x

26. Ocken H, Garbett K (2001) An evaluation of enriched boric acid in European PWRs. Electric Power Research Institute, EPRI Report, UK

27. Zhang W, Liu T, Xu J (2016) Preparation and characterization of 10B boric acid with high purity for nuclear industry. Springerplus 5:1202. https://doi.org/10.1186/s40064-016-2310-6

28. Blok J (2005) Update on use of enriched boric acid in domestic pressurized water reactors. Electric Power Research Institue, California

29. Zhang T, Li D, Meng L (2021) Recent progresses on the boron species in aqueous solution: structure, phase equilibria, metastable zone width (MZW) and thermodynamic model. Rev Inorg Chem 41:49–60. https://doi.org/10.1515/revic-2020-0012

30. Ge H, Zhou Y, Liu H, Fang Y, Fang C (2017) Molecular interactions in aqueous solutions of polyborates at different acidity based on the Raman spectroscopy data at 25 °C. Russ J Phys Chem A 91:1925–1931. https://doi.org/10.1134/S0036024417100119

31. Hirao T, Kotaka M, Kakihana H (1979) Raman spectra of polyborate ions in aqueous solution. J Inorg Nucl Chem 41:1217–1220

32. Hameed S, Awad HA, Al-Uqaily RAH (2020) Boron removal from seawater using adsorption and ion exchange techniques. Ecol Environ Conserv 26:480–487

33. He M, Xiao Y, Jin Z, Liu W, Ma Y, Zhang Y, Luo C (2013) Quantification of boron incorporation into synthetic calcite under controlled pH and temperature conditions using a differential solubility technique. Chem Geol 337–338:67–74. https://doi.org/10.1016/j.chemgeo.2012.11.013

34. Böhlke S, Schuster C, Hurtado A (2008) About the volatility of boron in aqueous solutions of borates with vapour in relevance to BWR-reactors. In: International conference on the physics of reactors "Nuclear power: A sustainable resource." Interlaken, Switzerland, pp 3089–3096

35. Kakihana H, Kotaka M, Satoh S, Masao N, Makoto O (1977) Fundamental studies on the Ion exchange separation of boron isotopes. Bull Chem Soc Jpn 50:158–163. https://doi.org/10.1246/bcsj.50.158

36. Parks JL, Edwards M (2005) Boron in the environment. Crit Rev Environ Sci Technol 35:81–114. https://doi.org/10.1080/10643380590900200

37. Kobayashi K, Hashimoto Y, Wang SL (2020) Boron incorporation into precipitated calcium carbonates affected by aqueous pH and boron concentration. J Hazard Mater 383:121183. https://doi.org/10.1016/j.jhazmat.2019.121183

38. Wang YJ, Wei HZ, Jiang SY, van de Ven TGM, Ling BP, Li YC, Lin YB, Guo Q (2018) Mechanism of boron incorporation into calcites and associated isotope fractionation in a steady-state carbonate-seawater system. Appl Geochem 98:221–236. https://doi.org/10.1016/j.apgeochem.2018.09.013

39. Yokozeki K (2007) Leaching from cementitious materials used in radioactive waste disposal sites. In: Letcher TM (ed) Thermodynamics, solubility and environmental issues. Elsevier, pp 169–186

40. Ekström T (2001) Leaching of concrete: experiments and modelling. LTH, Lund University

41. Babaahmadi A (2015) Durability of cementitious materials in long-term contact with water. Chalmers University of Technology, Sweden

42. Yokozeki K, Watanabe K, Sakata N, Otsuki N (2003) Prediction of changes in physical properties due to leaching of hydration products from concrete. J Adv Concr Technol 1:161–171. https://doi.org/10.3151/jact.1.161

43. Zheng Z, Li Y, Zhang Z, Ma X (2020) The impacts of sodium nitrate on hydration and microstructure of Portland cement and the leaching behavior of Sr^{2+}. J Hazard Mater 388:121805. https://doi.org/10.1016/j.jhazmat.2019.121805

44. Hwang E, Hwang S (1991) Effect of neutralizing agent content on 137-Cs leaching from solidified boric acid waste products. J Radioanal Nucl Chem 148:43–51. https://doi.org/10.1007/BF02060545

45. Sun Q, Li J, Wang J (2011) Effect of borate concentration on solidification of radioactive wastes by different cements. Nucl Eng Des 241:4341–4345. https://doi.org/10.1016/j.nucengdes.2011.08.040

46. Sun Q, Li J, Wang J (2011) Solidification of borate radioactive resins using sulfoaluminate cement blending with zeolite. Nucl Eng Des 241:5308–5315. https://doi.org/10.1016/j.nucengdes.2011.08.028

47. Hungarian Atomic Energy Authority (2017) Republic of Hungary, National report, Sixth Report prepared in the framework of the Joint Convention on the Safety of Spent Fuel Management and on the Safety of Radioactive Waste Management, Budapest

48. Masonnave JC (1993) Immobilization of borates and phosphates anions with saturated lime solutions. Solid State Ioncs 59(1–2):133–139

49. Huang C-T, Yang W (1994) A high volume efficiency process for solidification of boric acid wastes. In: The 4th international topical meeting on Nuclear thermal hydraulics operations and safety - Taipei - Taiwan. Taipei - Taiwan

50. Csetenyi LJ, Glasser FP (1995) Borate retardation of cement set and phase relations in the system Na_2O–CaO–B_2O_3–H_2O. Adv Cem Res 7:13–19. https://doi.org/10.1680/adcr.1995.7.25.13

51. Champenois JB, Dhoury M, Cau Dit Coumes C, Mercier C, Revel B, Bescop PL, Damidot D (2015) Influence of sodium borate on the early age hydration of calcium sulfoaluminate cement. Cem Concr Res 70:83–93. https://doi.org/10.1016/j.cemconres.2014.12.010

52. Tsuyumoto I, Oshio T, Katayama K (2007) Preparation of highly concentrated aqueous solution of sodium borate. Inorg Chem Commun 10:20–22. https://doi.org/10.1016/j.inoche.2006.08.019

53. Lahalle H, Cau Dit Coumes C, Mercier C, Lambertin D, Cannes C, Delpech S, Gauffinet S (2018) Influence of the w/c ratio on the hydration process of a magnesium phosphate cement and on its retardation by boric acid. Cem Concr Res 109:159–174. https://doi.org/10.1016/j.cemconres.2018.04.010

54. Aïtcin PC (2019) The influence of the water/cement ratio on the sustainability of concrete. In: Lea's chemistry of cement and concrete, fifth. Elsevier Ltd, pp 807–826

55. ASTM C1308-21 (2021) Standard test method for accelerated leach test for diffusive releases from solidified waste. ASTM International, West Conshohocken PA

56. Abdelrahman R, Zaki A, Elkamash A (2007) Modeling the long-term leaching behavior of ^{137}Cs, ^{60}Co, and [152,154]Eu radionuclides from cement–clay matrices. J Hazard Mater 145:372–380. https://doi.org/10.1016/j.jhazmat.2006.11.030

57. Osmanlioglu AE (2002) Immobilization of radioactive waste by cementation with purified kaolin clay. Waste Manag 22:481–483

58. Davraz M (2015) The effect of boron compound to cement hydration and controllability of this effect. Acta Phys Pol A 128:26–33

59. Boulard L, Kautenburger R (2020) Short-term elemental release from Portland cement concrete in hypersaline leaching conditions. Adv Cem Res 32:148–157. https://doi.org/10.1680/jadcr.18.00085

60. Yokozeki K, Watanabe K, Sakata N, Otsuki N (2004) Modeling of leaching from cementitious materials used in underground environment. Appl Clay Sci 26:293–308. https://doi.org/10.1016/j.clay.2003.12.027

61. Zhang W, Tang Y, Xu J (2018) Online determination of boron isotope ratio in boron trifluoride by infrared spectroscopy. Appl Sci (Switzerland) 8:1–10. https://doi.org/10.3390/app8122509

62. Abdel Rahman RO, Zaki AA, El-Kamash AM (2007) Modeling the long-term leaching behavior of ^{137}Cs, ^{60}Co, and [152,154]Eu radionuclides from cement-clay matrices. J Hazard Mater 145:372–380. https://doi.org/10.1016/j.jhazmat.2006.11.030

63. Revetegat E, Richet C, Gegout P (1992) Effect of Ph on the durability of cement pastes. Cement Concrete 22:259–272. https://doi.org/10.1016/0008-8846(92)90064-3

64. Zhou Y, Fang C, Fang Y, Zhu F (2011) Polyborates in aqueous borate solution: a Raman and DFT theory investigation. Spectrochim Acta A Mol Biomol Spectrosc 83:82–87. https://doi.org/10.1016/j.saa.2011.07.081

65. Applegarth LMSGA, Pye CC, Cox JS, Tremaine PR (2017) Raman spectroscopic and ab initio investigation of aqueous boric acid, borate, and polyborate speciation from 25 to 80 °C. Ind Eng Chem Res 56:13983–13996. https://doi.org/10.1021/acs.iecr.7b03316

66. Ge H, Zhou Y, Liu H et al (2017) Molecular interactions in aqueous solutions of polyborates at different acidity based on the Raman spectroscopy data at 25 °C. Russ J Phys Chem A 91:1925–1931. https://doi.org/10.1134/S0036024417100119

67. Zhou YQ, Fang CH, Fang Y, Zhu FY, Cao L (2012) Polyborates in aqueous sodium borate solution at 298.15 K. Asian J Chem 24:29–32

68. Thomas R (2002) Determination of the H_3BO_3 concentration in fluid and melt inclusions in granite pegmatites by laser Raman microprobe spectroscopy. Am Miner 87:56–68. https://doi.org/10.2138/am-2002-0107

69. Spessard JE (1970) Investigations of Borate equilibria in neutral salt Solutions Investigations of borate equilibria in aqueous salt solutions. J Inorg Nucl Chem 32:2607–2613. https://doi.org/10.1016/0022-1902(70)80308-6

70. Duffin AM, Schwartz CP, England AH, Uejio JS, Prendergast D, Saykally RJ (2011) PH-dependent x-ray absorption spectra of aqueous boron oxides. J Chem Phys 134:154503. https://doi.org/10.1063/1.3574838

71. Du Z, Chen J, Ye W, Guo J, Zhang X, Zheng R (2015) Investigation of two novel approaches for detection of sulfate ion and methane dissolved in sediment pore water using Raman spectroscopy. Sensors (Switzerland) 15:12377–12388. https://doi.org/10.3390/s150612377

72. Vibrations WM, Spectroscopy R (2022) PhysicsOpenLab water molecule vibrations with Raman spectroscopy. 1–10

73. Spectral Search | PublicSpectra. https://publicspectra.com/SpectralSearch. Accessed 6 Aug 2022

74. Furukawa T, White WB (1981) Raman spectroscopic investigation of sodium borosilicate glass structure. J Mater Sci 16:2689–2700. https://doi.org/10.1007/bf00552951

75. Gharavi-Naeini J, Yoo KW, Stump NA (2018) Characterization of barium borate frameworks using Raman spectroscopy. Appl Spectrosc 72:627–633. https://doi.org/10.1177/0003702817748952

76. Abramoff MD, Magalhaes PJ, Ram SJ (2004) Image Processing with ImageJ. Biophoton Int 11:36–42

77. Klochko K, Kaufman AJ, Yao W, Byrne RH, Tossell JA (2006) Experimental measurement of boron isotope fractionation in seawater. Earth Planet Sci Lett 248:276–285. https://doi.org/10.1016/j.epsl.2006.05.034

78. Kloppmann W, Petelet-Giraud E, Guerrot C, Cary L, Pauwels H (2015) Extreme boron isotope ratios in groundwater. Proced Earth Planet Sci 13:296–300. https://doi.org/10.1016/j.proeps.2015.07.069

79. Liu Y, Tossell JA (2005) Ab initio molecular orbital calculations for boron isotope fractionations on boric acids and borates. Geochim Cosmochim Acta 69:3995–4006. https://doi.org/10.1016/j.gca.2005.04.009

80. Mesmer RE, Baes CF, Sweeton FH (1972) Acidity measurments at elevated temperatures. Inorg Chem 11:537–543

81. Marschall H, Foster G (2018) Advances in isotope geochemistry-boron isotopes. Springer, Switzerland

82. Chen T, Lyu J, Wang Q, Bai P, Wu Y, Guo X (2021) Mechanistic study on boron adsorption and isotopic separation with magnetic magnetite nanoparticles. Mater Sci 56:4624–4640. https://doi.org/10.1007/s10853-020-05546-x

83. William Ed, White M (2016) Boron stable isotopes. In: Encyclopedia of geochemistry. Springer International Publishing, https://doi.org/10.1007/978-3-319-39193-9

84. Davraz M (2010) The effects of boron compounds on the properties of cementitious composites. Sci Eng Compos Mater 17:1–17. https://doi.org/10.1515/secm.2010.17.1.1

85. Vieira VM, Oliveira de Tello CC (2016) Study of chemical additives in the cementation of radioactive waste of PWR reactors. Univ J Chem 4:1–9

86. van Eijk RJ, Brouwers HJH (2000) Modelling the effects of waste components on cement hydration. Waste Manag Ser 1:685–694. https://doi.org/10.1016/S0713-2743(00)80078-1

87. Ojovan MI, Lee WE (2014) Immobilisation of radioactive waste in cement. In: An Introduction to nuclear waste immobilisation. Elsevier, pp 205–232. https://doi.org/10.1016/b978-0-08-099392-7058.00015-2

88. Saleh HE-D, Talat Bayoumi SE (2012) Characterizations of polyester-cement composites used for the immobilization of radioactive wastes. In: Saleh HM (ed) Polyester. IntechOpen, London, pp 257–290

89. Kamali S, Moranville M, Leclercq S (2008) Material and environmental parameter effects on the leaching of cement pastes: experiments and modelling. Cem Concr Res 38:575–585. https://doi.org/10.1016/j.cemconres.2007.10.009

90. Zhang SP, Zong L (2014) Evaluation of relationship between water absorption and durability of concrete materials. Adv Mater Sci Eng 2014:650373. https://doi.org/10.1155/2014/650373

91. Faucon P, Le Bescop P, Adenot F, Bonville P, Jacquinot JF, Pineau F, Felix B (1996) Leaching of cement: study of the surface layer. Cem Concr Res 26:1707–1715. https://doi.org/10.1016/S0008-8846(96)00157-3

92. Kochkodan V, Darwish NB, Hilal N (2015) The chemistry of boron in water. In: Boron separation processes, 1st edition. Elsevier, Swansea University, pp 35–63. https://doi.org/10.1016/B978-0-444-63454-7192.00002-2

93. Saleh HM, Shatta HA (2013) Immobilization of simulated borate radioactive waste solution in cement-poly(methylmethacrylate)

composite: mechanical and chemical characterizations. J Nucl Chem 2013:1–7. https://doi.org/10.1155/2013/749505

94. Zhang W, Wang J (2017) Leaching performance of uranium from the cement solidified matrices containing spent radioactive organic solvent. Ann Nucl Energy 101:31–35. https://doi.org/10.1016/j.anucene.2016.09.055